Optimal Micro-siting of Wind Turbines in an Offshore Wind Farm Using Frandsen-Gaussian Wake Model

Siyu Tao, *Student Member, IEEE,* Stefanie Kuenzel, *Member, IEEE,* Qingshan Xu, *Member, IEEE,* and Zhe Chen, *Fellow, IEEE*

***Abstract*—This paper proposes a method to obtain the optimal placement of wind turbines (WTs) in an offshore wind farm (WF). The optimization objective is to minimize the levelized average cost per net electric power generated by a WF with a fixed number of WTs while the distance between WTs is not less than the allowed minimal distance in the far wake region. The WT wake losses have been taken into account, with the Frandsen-Gaussian (F-G) wake model and the optimization problem is subsequently solved by the Hybrid Grey Wolf Optimization (HGWO) algorithm. Synthesis methods which contain a special WT ranking strategy for multiple WTs are described in detail. Both the F-G model and Jensen's model are applied in the offshore WF optimization simulation platform for comparison. Simulation results demonstrate that the F-G model is more consistent with real wakes and thus the optimization result is more accurate than the commonly used Jensen's model.**

***Index Terms*—Frandsen-Gaussian wake model, Hybrid Grey Wolf Optimization algorithm, micro-siting, offshore wind farm planning, optimization, wake effect**

I. Introduction

VARIOUS national and international initiatives for generating electrical power from sustainable sources have driven an unprecedented growth in wind energy development. As is predicted, the world will have over 800 GW of installed wind generator capacity by 2020 [1]. The optimal micro-siting of WTs which plays a key role in maintaining the balance between investment and electricity generation has been a challenge for both onshore and offshore WFs. With the best wind resources largely being over water and land being more extensively exploited for onshore WFs, offshore WF development is currently recognized to be the promising choice. As constructing and operating offshore WFs is more challenging and more expensive [2], it is imperative to design the offshore WF layout and to select the WT location and size for producing maximum power output under widely varying wind speeds and directions.

It is a complicated task to mathematically model a WF for the optimization problem and the computation time is usually very long to solve this problem mainly due to the iterative calculations of the velocity deficit caused by WTs which is known as wake effect [3]. An upwind WT extracts energy from wind and forms a wake that results in the reduced wind speed and increased level of turbulence at the downwind WTs. The downwind WTs produce less power and suffer increased fatigue loads if they are affected by the wake. This phenomenon is most obvious for large WFs where WTs are installed in a group or a cluster. Since the energy available in the wind is a cubic function of the wind speed, an inaccurate evaluation of the velocity field in a WF can lead to large errors in the forecasting of the energy output [4]. Thus, it is necessary and beneficial to establish an accurate analytical wake model for the WT micro-siting problem.

Many scholars have studied the analytical modeling of wake effect. In 1983, Jensen [5] put forward a simple wake model by conservation of mass for the first time which is known as the Park model. Jensen's model assumes that the wake expands linearly after a WT which is regarded as a one-dimensional (1-D) wake model. Katic *et al.* [6] refined this model in 1986 by considering the axial induction factor. So far, because of its simplicity, Jensen's model and its refined model have become a preferential option to be widely applied in the WT optimal micro-siting simulation problems [7] not only in the seminal research done by Mossetti *et al.* [3] in 1994, Grady *et al.* [8] in 2005 and Sisbot *et al.* [9] in 2009 but also in the majority of recent literature [10-16]. In addition, Jensen's model has been extensively applied in the commercial WF planning software, *e.g.*, WAsP [17], WindFarmer [18], WindSim [19], and OpenWind [20]. In 1988, Larsen [21] constructed a semi-analytic wake model which is recommended for solving the wake loading problem. In 2006, Frandsen [22] proposed a simplified model by conservation of momentum which is justified to be more accurate than the previous ones. This model is applied in the optimization of a WF layout as well [23]. Other well-known 1-D wake models include the Ishihara model [24], and the model by Yang and Sotiropoulos [25], *etc.* However, in the 1-D wake models, at any particular downstream distance, the inside wind velocity is seen to be constant across the wake plane and has a top-hat shape profile. This is far from reality where the velocity deficit profile possesses a Gaussian shape. To address the deficiencies of the 1-D wake models, in 2014 Bastankhah and Porté-Agel [26] proposed a two-dimensional (2-D) Gaussian wake model which is superior to Jensen's model. Recently, some other 2-D wake models were developed such as the Cosine wake model developed by Tian *et al.* [27] in

S. Y. Tao and Q. S. Xu are with the Department of Electrical Engineering, Southeast University, Nanjing, 210096, China, (e-mail: 230188145@seu.edu.cn; xuqingshan@seu.edu.cn).

S. Kuenzel is with the Department of Electronic Engineering, Royal Holloway, University of London, Egham, TW20 0EX, U.K. (e-mail: Stefanie.Kuenzel@rhul.ac.uk).

Z. Chen is with the Department of Energy Technology, Aalborg University, Aalborg, 9220, Denmark, (e-mail: zch@et.aau.dk).

2015 and the Jensen-Gaussian (J-G) wake model proposed by Gao *et al.* [28] in 2016. The 2-D wake models have been justified to be more effective in predicting wind deficits than the 1-D wake models.

In order to take advantage of the aforementioned 2-D wake model [26], and also to avoid the adverse effects of the single crude wake model frequently used for the WT optimal micro-siting problem, a compounded 2-D wake model of high accuracy *i.e.* the F-G model is utilized in this work. It is a combination of Frandsen's model and the Gaussian wake model which are based on the law of conservation of mass and momentum. A better optimization algorithm in a continuous search space is implemented to solve the WT micro-siting problem.

This paper is arranged as follows: In Section II the F-G wake model is presented and validated; in Section III the overall mathematical model of the optimization problem is proposed; Section IV introduces the optimization algorithm: the HGWO algorithm. Section V discusses the simulation results followed by Section VI, the conclusion.

II. Analytical Model Of Wake

A. General Characteristics of Wake Effect

Wake effect is one of the most important influences of adjacent WTs that impact the electric energy production. Due to wake effect, the power produced by a WF is lower than what would be produced by the sum of the equivalent number of single WTs without wake effects. It is estimated that about 10-20% of the total power of a WF is lost on this account [28]. Thus, when WFs are designed, a trade-off between the losses in wind generation through the wake effect and the cost of spacing the WTs farther apart has to be made.

The wake affected area behind a WT is usually divided into two parts, *i.e.* the near wake region and the far wake region. As denoted in Fig. 1-Fig. 3, supposing the location of WT to be x=0, the region between the dash lines A and B ($0<x<x_1$) is a perturbed region which is the so-called near wake region. The region outside line B ($x>x_1$) is called far wake region. Line B is defined by the pressure, *i.e.* the pressure on line A and line B almost equals to the ambient pressure p_0 [29]. Usually, $x_1=3d_r$, where d_r is the rotor diameter of the WT.

B. Comparison of Jensen's Model and Frandsen's Model

Jensen's model (Fig. 1) is derived based on the actuator disk model [5] which assumes that the control volume composes a fluid tube. Based on conservation of mass, it is assumed that:

$$\rho\pi r_2^2 v_2+\rho\left(\pi r_x^2-\pi r_2^2\right)v_0=\rho\pi r_x^2 v_x \tag{1}$$

where ρ is the air density, v_0 is the ambient wind speed, r_2 is the downstream radius, r_x is the wake radius at the distance x, v_2 and v_x are the correspondent wind speeds.

Jensen's model assumes that the far wake region is a cone and has a top-hat shape. On each intersection perpendicular to the cone's axis, the wind velocities are identical, pointing to the direction of the air flow and can be expressed by (2) [5].

$$v_x=v_0\left[1-\left(1-\sqrt{1-C_T}\right)\left(\frac{r_2}{r_2+k_{wake}x}\right)^2\right] \tag{2}$$

where k_{wake} is the wake expansion rate and C_T is the thrust coefficient, and is defined as follows.

$$C_T=T/T_m \tag{3}$$

where T is the thrust force exerted by the wind on the actuator disk and T_m is the theoretical maximum thrust force.

$$T_m=\frac{1}{2}\rho\pi r_r^2 v_0^2 \tag{4}$$

where r_r is the WT rotor radius.

Frandsen's model (Fig. 2) is deduced according to the blade element momentum theory [22] which considers the details of blades and offers a commendable evaluation for torques and thrust forces. Based on the conservation of momentum, it is assumed that:

$$\left(\rho\pi r_x^2 v_x\right)\left(v_0-v_x\right)=T \tag{5}$$

The wind speed at the distance x in Frandsen's model is given as follows [22].

$$v_x=v_0\left[1-\frac{1}{2}\left(1-\sqrt{1-\frac{2C_T}{\left(r_x/r_r\right)^2}}\right)\right] \tag{6}$$

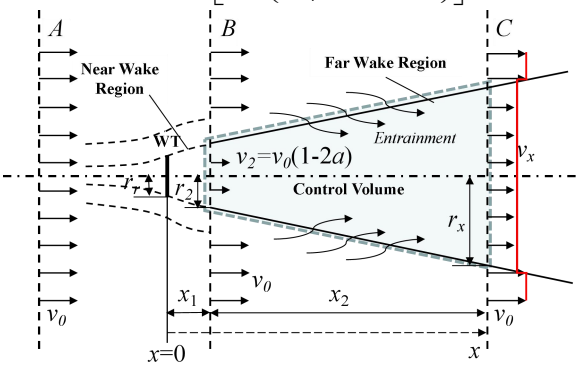

Fig. 1. Jensen's model [5].

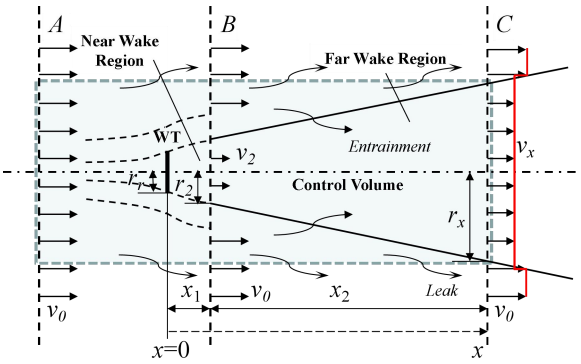

Fig. 2. Frandsen's model [22].

Both models hold distinct characteristics. Firstly, the patterns of recovery along the axis are different in the two models. This is mainly because Jensen's model is based on the conservation of mass, while Frandsen's model is not only based on the conservation of mass but it also considers the conservation of momentum. Limited by the simplified assumptions in the actuator disk model, it is unable to simultaneously meet both conservation. Secondly, Jensen's model is based on the distribution at the exit of the near wake region (indicated by r_2 in (2)), while Frandsen's model fully includes the near wake region (indicated by r_r in (6)) and has a global vision. On this account, Frandsen's model outperforms Jensen's model to a

certain extent. However, both models share a common demerit which is an even distribution of wind speed on every cross section that is assumed to form a cone. This is not congruent with the real case and will overestimate the wind speed in the wake. Thus, neither of them is able to give an accurate prediction.

In view of the above, in this work a Gaussian wake model on the basis of Frandsen's model is derived that not only takes advantage of Frandsen's model, but also overcomes the common shortcomings of the 1-D wake models. In addition, Jensen's model is set to be a reference for comparison.

C. The F-G Wake Model

The F-G model proposed firstly in [26], is demonstrated in Fig. 3. Unlike the aforementioned models, the boundary of the far wake region is not confined, but infinite (denoted by dotted lines in Fig. 3). This model assumes that wind speed in the far wake region depends on two variables, *i.e.* x and r. x is the distance from the first WT and r is the distance from the axis of the WT. The near wake region is also included.

The Gaussian wake model assumes that [26]:

$$v_{x,r}=\left[1-K(x)\exp\left(-\frac{r^2}{2\sigma^2}\right)\right]v_0 \tag{7}$$

It holds for all $x>x_1$ and $r\geq 0$. $v_{x,r}$ is the wind speed at distance x, radius r. σ is the standard deviation of the distribution which is denoted characteristic width in this paper. $K(x)$ is an undetermined coefficient of x.

In Frandsen's model the mass flow rate $\dot{m}$ is supposed to be [22]:

$$\dot{m}=\int_0^{+\infty}\rho v_{x,r}2\pi r dr \tag{8}$$

By the conservation of momentum, it can be obtained that:

$$\int_0^{\infty}\rho v_{x,r}\left(v_0-v_{x,r}\right)2\pi r dr=T \tag{9}$$

which can be rewritten as (10).

$$K^2(x)-2K(x)+\frac{C_T}{2(\sigma/r_r)^2}=0 \tag{10}$$

Solving (10) and adopting the physically feasible root, the following solution is obtained.

$$K(x)=1-\sqrt{1-\frac{C_T}{2(\sigma/r_r)^2}} \tag{11}$$

This model assumes that σ is a linear function of x as well. On every plane orthogonal to the axis, the mass flow rate of the F-G model is the same as that of its corresponding Frandsen's model which implies [26]:

$$\int_0^{r_x}\rho\left[1-\frac{1}{2}\left(1-\sqrt{1-\frac{2C_T}{(r_x/r_r)^2}}\right)\right]v_0 2\pi r dr+\int_{r_x}^{\infty}\rho v_0 2\pi r dr$$
$$=\int_0^{\infty}\rho v_{x,r}2\pi r dr \tag{12}$$

Substituting (11) into (7), replacing the resulting equation into (12), solving and simplifying, finally (13) is obtained.

$$\sigma=\frac{r_x}{2}=\frac{r_0}{2}+\frac{\alpha}{2}x \tag{13}$$

where r_0 is the actuator disk radius and α the entrainment constant. They are empirically given as [4][26]:

$$r_0=0.8r_2 \tag{14}$$

$$\alpha=\frac{0.56}{\ln(z_h/z_0)} \tag{15}$$

where z_h is the WT hub height and z_0 is the surface roughness length.

Equations (7), (11) and (13) are the basic equations of the F-G model.

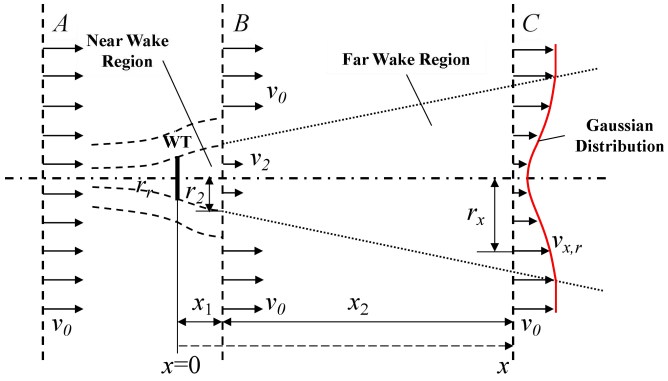

Fig. 3. The F-G model [26].

D. Validation of the F-G Wake Model

To verify the performance of the F-G model, a series of comparisons are given among Jensen's model, Frandsen's model and their Gaussian variations.

Fig. 4 demonstrates the velocity curves of the aforementioned wake models compared with wind tunnel measured data [28] at the downwind distances $x=2.5d_r$, $x=5d_r$ and $x=10d_r$ respectively. Firstly, it can be clearly observed that Jensen's model and Frandsen's model share the same characteristic top-hat shape. Secondly, it can be seen that when $r=0$, the deficit of the F-G model is twice as large as that of Frandsen's model. This phenomenon is a consequence of equal flow of mass and momentum. That is to say, on every plane orthogonal to the axis, the rate of flow of mass and the momentum of the F-G model is equal to that of its relevant Frandsen's model. Furthermore, compared with other wake models, the F-G model holds the best prediction performance which fits best with the wind tunnel measured data not only in the near wake region ($x=2.5d_r$), but also in the far wake region ($x=5d_r$, $x=10d_r$).

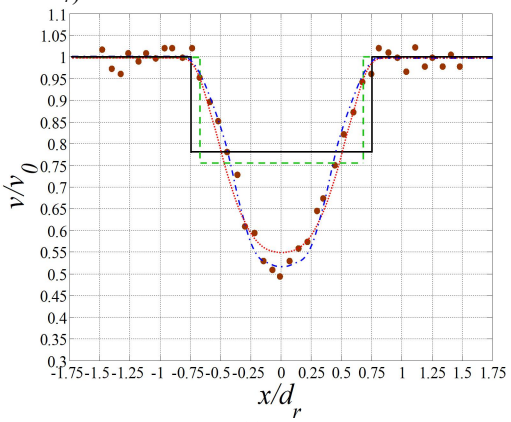

(a)

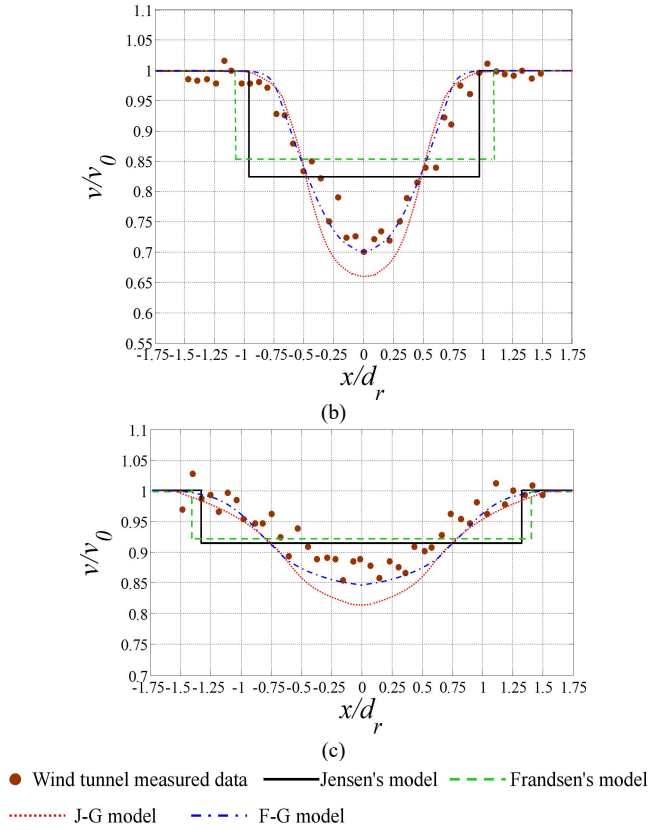

Fig. 4. Comparison of different wake models' predicted velocities and wind tunnel measurement data [28] at specific downwind distance. (a) x=2.5d_r. (b) x=5d_r. (c) x=10d_r.

Large-Eddy Simulation (LES) is proven to have the ability of producing the magnitude and spatial distribution of the most relevant turbulence statistics of WT wakes in turbulent boundary layer flows [30]. The maximum wind deficit ratio of the four types of wake models and the LES data [26] are given in Fig. 5 for comparison. This figure demonstrates that Jensen's model and Frandsen's model underestimates the maximum velocity deficit while the J-G model [28] overestimates the maximum velocity deficit in the region of $2d_r \le x \le 16d_r$ with respect to the LES data. It also shows that the F-G model has the best performance not only for the onshore scenario (Fig. 5(a)), but also for the offshore scenario (Fig. 5(b)), if relative parameters can be accurately determined through fitting experimental results. This confirms the F-G model is well suited for the study of onshore as well as offshore WFs.

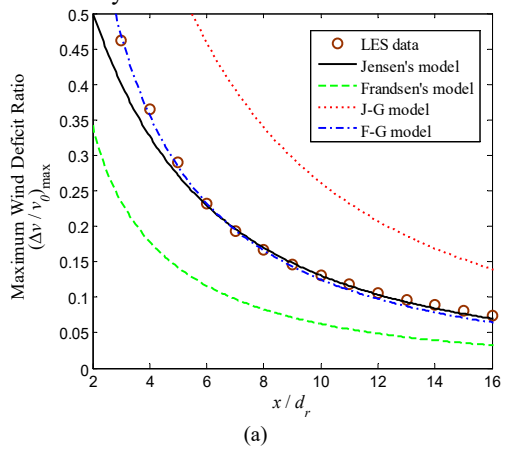

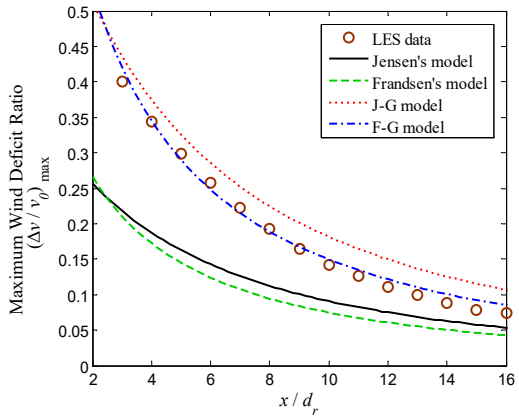

Fig. 5. Comparison of different wake models with LES data [26] using normalized velocity deficit versus normalized downwind distance. (a) onshore scenario (z_0=0.3m). (b) offshore scenario (z_0=0.0002m).

D. Synthesis Methods for Wakes of Multiple WTs

1) The Second Norm Method (SNM)

Taking the parallel scenario in Fig. 6 as an example, it is assumed there are n WTs T_i (i=1, 2, ..., n) in front of T_j. The SNM [5] is applied to synthesize the deficit ratio of the wind speed in front of T_j, *i.e.* $a_{v,j}$, as follows.

$$a_{v,j} = \sqrt{\sum_{i=1}^{n} a_{vi,j}^2} \tag{16}$$

$$a_{vi,j} = \frac{v_0 - v_{i,j}}{v_0}, \quad i = 1,2,\cdots,n \tag{17}$$

where $v_{i,j}$ is the wind speed in front of T_j when only T_i (i=1, 2, ..., n) and T_j exists and $a_{vi,j}$ is the deficit ratio of each wind speed accordingly which is also called axial induction factor.

Knowing the deficit ratio, the wind speed in front of each WT can be subsequently calculated.

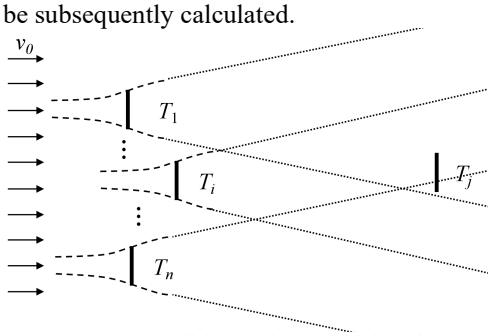

Fig. 6. A parallel scenario of multiple wakes.

2) The Multiplication Method (MPM)

Taking the cascaded scenario in Fig. 7 as an example, it is assumed there are n WTs T_i (i=1, 2, ..., n) in front of T_j. The MPM [5] states that:

$$v_j = v_0 \prod_{i=1}^{n} \left(1 - \frac{2a_i}{\left(1 + \alpha\left(x_{i,j} / r_{2,i}\right)\right)^2} \right) \tag{18}$$

where a_i is the axial induction factor of T_i. $r_{2,i}$ is the corresponding value of r_2 of T_i and $x_{i,j}$ is the distance between T_i and T_j, as illustrated in Fig. 7.

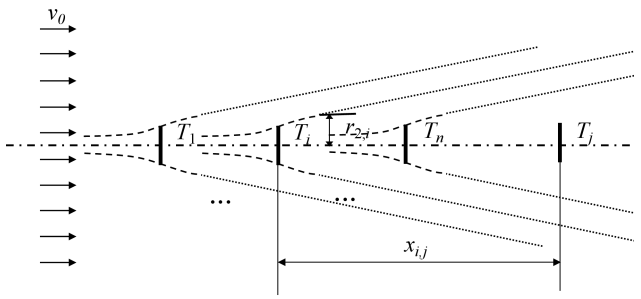

Fig. 7. A cascaded scenario of multiple wakes.

3) Ranking WTs

For demonstration, Fig. 8 shows an array of 12 WTs, namely T_1, T_2, …, T_{12}. Supposing wind comes from the west, the WTs which are not in the wake of any other WTs are defined as seeding WTs and the rank of those WTs are set to be 1. A set R_1={T_1, T_2, T_3, T_4} is formed accordingly. The rank of those WTs which are only in the wake of seeding WTs are taken to be 2 and R_2={T_5, T_6, T_7, T_8}. For the same token, WTs that are only in the wakes of WTs in R_1 and R_2 are of rank 3 and R_3={T_9, T_{10}, T_{11}, T_{12}}. Rank 4, 5 and so forth can be determined likewise.

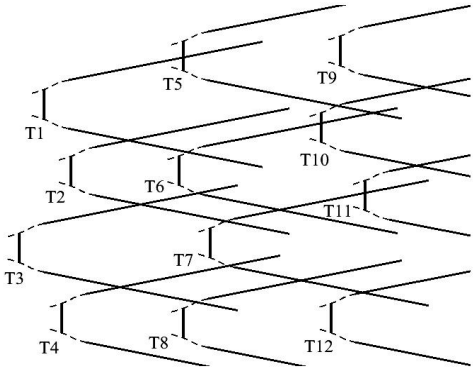

Fig. 8. Demonstration of WTs' ranking.

In Frandsen's model, the wake's boundary is well defined. If a part of T_2 touches the wake of T_1, it means T_2 is in the wake of T_1. If T_2 is not completely emerged in the wake of T_1, the partial coverage algorithm is involved. In the Gaussian wake model, the wake's boundary takes 3σ line as the recommended value [26]. An advantage of the Gaussian wake model is that the transition of boundaries is smooth whereas other models involve partial coverage algorithms and the transition of boundaries is abrupt. For the Gaussian wake models, if the center of T_2 is in the wake of T_1, it is regarded to be in the wake of T_1, otherwise not. Obviously, it is easier to decide if a WT is in the wake of another in the Gaussian wake model.

4) Algorithm for Ranking

When performing ranking, the first problem to be tackled is to judge whether a WT is in the wake of another. The coordinates of T_1 and T_2 are supposed to be (x_1,y_1) and (x_2,y_2). The actual shape of T_1's wake is complicated, and relies on wind speed and direction. The case in Fig. 9 is taken for illustration. Firstly, given the direction of the ambient wind θ, the unit vector that represents the direction of the ambient wind is $\mathbf{e}=(\cos\theta, \sin\theta)$. The displacement vector of T_2 with respect to T_1 is constructed as $\mathbf{s}=(x_2-x_1, y_2-y_1)$. The projection of $\mathbf{s}$ on $\mathbf{e}$, which is denoted by s_0 in Fig. 9 is given as (19).

$$s_0 = (x_2-x_1)\cos\theta + (y_2-y_1)\sin\theta \tag{19}$$

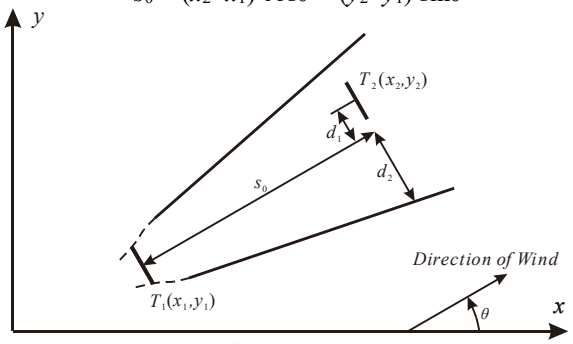

Fig. 9. Illustration of two WTs.

If $s_0 \le 0$, T_2 can never be in the wake of T_1. If $s_0>0$, d_1 and d_2 in Fig. 9 need to be calculated. d_1 can be obtained from (20).

$$d_1 = \sqrt{(x_2-x_1)^2 + (y_2-y_1)^2 - s_0^2} \tag{20}$$

In the F-G wake model d_2 is determined by (21).

$$d_2 = 3\sigma = 3(k^* s_0 + \sigma_0) \tag{21}$$

where k^* is the growth rate of σ, and σ_0 is the limit when x approaches 0, which are determined by (22) and (23).

$$k^* = \frac{0.28}{\ln(z_h/z_0)} \tag{22}$$

$$\sigma_0 = 0.4 r_r \sqrt{\frac{1-a}{1-2a}} = 0.4 r_2 \tag{23}$$

For $d_1 \le d_2$, T_2 is in the wake of T_1, otherwise not. It should be noted that when calculating σ_0, the axial induction factor a requires to be known, which is difficult to determine. As an approximation, the input wind speed on T_1 is assumed to always equal to v_0 when ranking WTs for the first time.

When ranking WTs, each pair of WTs are firstly compared and the results are stored in a table that contains all the identifications of WTs. The WTs in the table that are not in the wake of any other WT are designated R_1 and will be eliminated in the array. This process is continued until there is no WTs left in the array.

5) Implementation of the Methods

For the WT array shown in Fig. 8, the output power of R_1 WTs can be determined directly, as the wind speed is v_0.

For R_2 WTs, the deficit of wind can be determined using the SNM.

For R_3 WTs, the calculation of the wind deficits is more involved. For example, the deficits at T_9 due to R_1 WTs are synthesized by the SNM. Then, its equivalent wind speed can be calculated using the MPM, supposing the ambient wind speed to be v_0. This equivalent wind speed is taken to be v_0 for T_9. The deficits at T_9 due to R_2 WTs are calculated and all the deficits are synthesized by the SNM. Then its corresponding wind speed can be calculated, taking the aforementioned equivalent wind speed as its ambient wind speed. For WTs of higher ranks, like R_4, R_5 and so forth, the wind speeds can be determined likewise.

The proposed method mixes the SNM and the MPM, for the MPM cannot tackle parallel multiple WTs and the SNM neglects the cascaded effect when WTs are in a cascade.

III. Problem Definition

A. Objective Function and Constraints

The primary purpose of building a WF is to supply as much electricity as possible within a limited planning area. Meanwhile, the total investment demands to be reduced during the WF's whole lifetime. The levelized cost of energy (LCOE) is defined as the production cost of each unit of electricity generated during the WF working life including capital investment and lifetime running costs [31]. It can provide a good reference for WF planners to make a decision. In this way, the optimization problem can be described as a minimization of the annualized LCOE of the WF with constraints and can be stated as (24).

$$\begin{aligned} &Min\ \ Obj:\ \ LCOE=\frac{CAPEX\cdot CRF+OPEX_{annual}}{AEP} \\ &s.t.\begin{cases} x_{\min}\le x_i\le x_{\max} & i=1,2,\cdots,N_t \\ y_{\min}\le y_i\le y_{\max} & i=1,2,\cdots,N_t \\ (x_i-x_j)^2+(y_i-y_j)^2\ge(5d_r)^2 & i,j=1,2,\cdots,N_t,i\ne j \end{cases} \end{aligned} \tag{24}$$

where $CAPEX$ [€] represents the capital expenditure, CRF is the capital recovery factor, $OPEX_{annual}$ [€/year] is the annualized operation and maintenance (O&M) cost, AEP [MWh] is the annual energy production of the WF, (x_i, y_i) is the position of the i-th WT with the boundary of the WF to be $[x_{min}, x_{max}]$ and $[y_{min}, y_{max}]$, N_t is the number of installed WTs.

The objective function is mainly formulated as a function of levelized annual total cost and AEP of the WF. It takes both electrical and economic factors into account which can be used to calculate the variation of the investment during the WF lifetime.

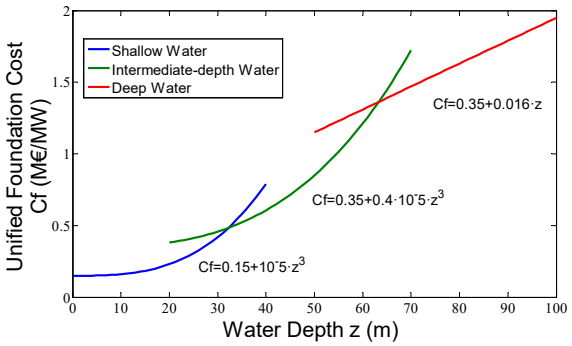

Fig. 10. The relationship between foundation cost and water depth [23].

The estimation of $CAPEX$ for the whole WF is expressed as (25) which takes two economic factors into consideration, one being total cost of WTs and the other foundation cost.

$$CAPEX=CAPEX_{WT}\cdot C\cdot N_t+\sum_{i=1}^{N_t}C_{fd,i}\left(z_i\left(x_i\right)\right) \tag{25}$$

The first term is the total capital expenditure on WTs, where $CAPEX_{WT}$ [M€/MW] denotes the capital cost per MW of the WTs, C [MW] is the WT's capacity. For an offshore WF, the second term represents the total construction cost of the foundations, where $C_{fd,i}$ [M€/MW] is the cost of the i-th WT's foundation which is a function of the water depth at the WT's location $z_i(x_i)$ [32]. A foundation cost versus water depth function can be devised and it is usually a piece-wise function [23] (Fig. 10). For the area where there are two options of foundations (20 m<z<40 m, 50 m<z<70 m), the cheaper one will be chosen. In the simulation, x=0 is set as the location of 40 km from the shore where the water depth is 12 m. $z_i(x_i)$ is supposed to be in a linear relationship with the distance from the shore, as given by (26).

$$z\left(x\right)=0.001x+12 \tag{26}$$

According to [23], the cost of substation and electricity infrastructure such as cables accounts for around 15-30% of an offshore WF's total cost. There can be various inner electrical distribution installation patterns such as ring structure, string structure and multi-loop structure *etc.* [33] which has a direct influence on the project cost and electrical losses. Due to the expensive cost of the offshore cable system, in practice, only simple and cheap topology are currently used. In order to compare the effectiveness of wake models, cable layout will not be taken into consideration in this study.

CRF is a function of the discount rate r [%] and the WF's lifetime N [year].

$$CRF=r/\left[1-\left(1+r\right)^{-N}\right] \tag{27}$$

The $OPEX_{annual}$ is defined as:

$$OPEX_{annual}=OPEX_{unit}\cdot C\cdot N_t \tag{28}$$

where $OPEX_{unit}$ [€/kW/year] is the annual O&M cost of unit electricity.

AEP is the product of the WF expected total output power, denoted as $E(P_{total})$ [MW] and the total hours in one year, denoted as T [h]. The power generated by each WT under the wind inflow condition can be computed based on the power curve of the WT. Combined with the probability distribution function (PDF) of the wind condition, AEP can be written as:

$$AEP=T\cdot E\left(P_{total}\right)=T\cdot\sum_{i=1}^{N_t}\sum_{j=1}^{M}f_j\left(\theta\right)\int_{v_{ci}}^{v_{co}}P_i\left(v_i\right)\cdot pdf_j\left(v,\theta\right)dv \tag{29}$$

where M is the total number of intervals with equal width into which the wind direction is discretized, $P_i(v_i)$ is the power curve function of the i-th WT, v_i is the wind speed the i-th WT experiences, $pdf_j(v, \theta)$ is the PDF of wind speed and wind direction for the j-th wind direction, $f_j(\theta)$ is the frequency of occurrence for the j-th wind direction, v_{ci} and v_{co} are the WT cut in and cut out wind speeds.

There are three constraints in this optimization problem. The first two constraints represent the feasible domain of each WT's location. In this study, the planning area is set to be a 5 km by 5 km square. In this way, the constraints of each WT's coordinates are as below:

$$x_i,y_i\in\left[0,5000\,m\right],\ \ \forall i=1,2,\cdots,N_t \tag{30}$$

The third constraint is the minimum distance between any two adjacent WTs:

$$\left(x_i-x_j\right)^2+\left(y_i-y_j\right)^2\ge\left(5d_r\right)^2,\ \ \forall i,j=1,2,\cdots,N_t,i\ne j \tag{31}$$

Here the minimum distance between any pair of WTs is set to be $5d_r$ to avoid high wake losses and excessive loads on the WTs caused by high levels of turbulence in the near wake region (x<3d_r).

B. Wind Scenario

For any geographical location, wind direction and speed are not constant. Fig. 11 demonstrates the probability distribution of wind speed's magnitude and direction profile of the planning area (measured at 10 km to the shore) in a form of a wind rose. It provides frequency of occurrence for wind in 36 directions (M=36), *i.e.* $f_j(\theta)$ in (29) for the j-th direction.

However, this distribution is quite crude. In this paper, overall wind behavior is characterized by the Weibull distribution for each wind direction [11][34] which is a widely accepted model to characterize the wind speed behavior, such as expressed in (32).

$$pdf(v,\theta)=\frac{k(\theta)}{c(\theta)}\left(\frac{v}{c(\theta)}\right)^{k(\theta)-1}\exp\left(-\left(\frac{v}{c(\theta)}\right)^{k(\theta)}\right) \quad (32)$$

where v [m/s] is the wind speed, $k(\theta)$ is the shape parameter and $c(\theta)$ [m/s] is the scale parameter. Both k and c are functions of the wind direction θ.

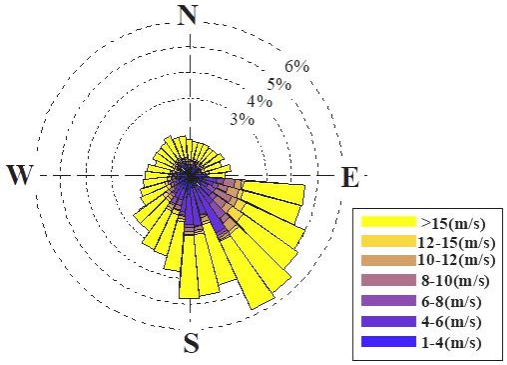

Fig.11. Wind rose [35].

In addition, for the offshore WF, when it gets farther from the shore, the wind speed increases accordingly [36]:

$$v(x)=v_{10}\cdot\left(-0.25\cdot e^{(-x/23)}+1.17\right) \quad (33)$$

where x [km] is the distance to the shore, v_{10} is the wind speed measured at 10 km to the shore and $v(x)$ is the wind speed at x.

IV. Optimization Algorithm

A. The HGWO Algorithm

The HGWO algorithm is a novel intelligence algorithm [37][38] which exploits the advantages of the Grey Wolf Optimization (GWO) algorithm and the Genetic Algorithm (GA) and uses a nonlinear control parameter to guarantee a more rapid convergence rate of the iteration. Based on the HGWO algorithm, an effective and efficient optimization platform is developed for the optimal micro-siting of WTs.

In the GWO algorithm, there are three kinds of wolves: α, β, δ which are the best, the second-optimal and the third-optimal solutions of the optimization problem. The grey wolves update their positions as follows to encircle the prey [37][38].

$$\vec{X}(t+1)=\vec{X}_p(t)-\vec{A}\otimes\vec{D} \quad (34)$$

$$\vec{D}=\left|\vec{C}\otimes\vec{X}_p(t)-\vec{X}_i(t)\right| \quad (35)$$

where t is the current iteration, $\vec{X}$ and $\vec{X}_p$ are the position vectors of a grey wolf and the prey respectively, $\vec{D}$ is the distance vector between the grey wolf and the prey. The operator $\otimes$ represents element-wise multiplication. The parameter vectors $\vec{A}$ and $\vec{C}$ are computed as follows:

$$\vec{A}=a\left(2\cdot\vec{r}_1-\vec{1}\right) \quad (36)$$

$$\vec{C}=2\cdot\vec{r}_2 \quad (37)$$

where $\vec{r}_1$ and $\vec{r}_2$ are the vectors of random numbers in the range of [0, 1], with the same dimensions of $\vec{X}$ and $\vec{X}_p$. $\vec{1}$ represents the vector whose elements all equal one.

Based on a nonlinear control parameter which is a cosine function, the adaptive parameter a is calculated as follows.

$$a=1-\cos\left(\left(1-t/t_{\max}\right)^k\cdot\pi\right) \quad (38)$$

where k is the nonlinear adjustment parameter and t_{max} is the maximum iteration time.

Using the positions of the α, β, δ wolves, each wolf updates its position according to the following formulae [37].

$$\begin{cases}\vec{D}_\alpha=\left|\vec{C}_1\otimes\vec{X}_\alpha(t)-\vec{X}(t)\right|\\ \vec{D}_\beta=\left|\vec{C}_2\otimes\vec{X}_\beta(t)-\vec{X}(t)\right|\\ \vec{D}_\delta=\left|\vec{C}_3\otimes\vec{X}_\delta(t)-\vec{X}(t)\right|\end{cases} \quad (39)$$

$$\begin{cases}\vec{X}_1=\vec{X}_\alpha(t)-\vec{A}_1\otimes\vec{D}_\alpha\\ \vec{X}_2=\vec{X}_\beta(t)-\vec{A}_2\otimes\vec{D}_\beta\\ \vec{X}_3=\vec{X}_\delta(t)-\vec{A}_3\otimes\vec{D}_\delta\end{cases} \quad (40)$$

$$\vec{X}(t+1)=\frac{1}{3}\sum_{m=1}^{3}\vec{X}_m \quad (41)$$

As shown in Fig. 12, the HGWO algorithm absorbs the cross-over and mutation operation of the GA to avert premature convergence and falling into a local minimum.

The probabilities of cross-over P_c and mutation P_m are as below.

$$P_c=\begin{cases}0.75-\dfrac{1}{|f_{best}-f_{mean}|}, & |f_{best}-f_{mean}|>\varepsilon_1\\ 0.5, & else\end{cases} \quad (42)$$

$$P_m=\begin{cases}0.075-\dfrac{1}{|f_{best}-f_{mean}|}, & |f_{best}-f_{mean}|>\varepsilon_2\\ 0.05, & else\end{cases} \quad (43)$$

where f_{best} and f_{mean} are the best and average values of the fitness of the current population respectively, ε_1 and ε_2 are accuracy parameters.

The new individuals are created as follows after the cross-over operation.

$$X'=\lambda_1\cdot X_a+(1-\lambda_1)\cdot X_b \quad (44)$$

where X_a and X_b are the positions of the parents, X' is the position of the newborn individual, λ_1 ($0\leq\lambda_1\leq1$) is a random parameter.

The whole population is generated after the mutation operation according to the following equation.

$$X''=X_i\cdot(1+\lambda_2)^m \quad (45)$$

where X'' is the position of the new individual after mutation, m is a control parameter, λ_2 ($0\leq\lambda_2\leq1$) is a random parameter.

B. Application of the HGWO Algorithm in the WT Optimal Micro-siting Problem

Fig. 12 illustrates the detailed procedure of the HGWO algorithm's application in the WT optimal micro-siting problem. The inputs are the data of the WF, wind condition, and the parameters of the HGWO algorithm, *etc*. When the WF contains N_t WTs, the variables are represented by the grey wolf's position vector $\vec{X}$ with the dimension of $2N_t$, indicating the x- and y- coordinates of the N_t WTs. Since the minimum and maximum values of the variables depend on the boundaries of

the WF, the range of each variable is [0,5000 m]. The outputs are the *x*- and *y*- coordinates of the N_t WTs when the grey wolves get the prey (*i.e.* the solution of the optimization problem). The minimum objective function solution is the final choice of WTs' layout. The optimization process ends if the best solution fitness remains the same for 800 generations.

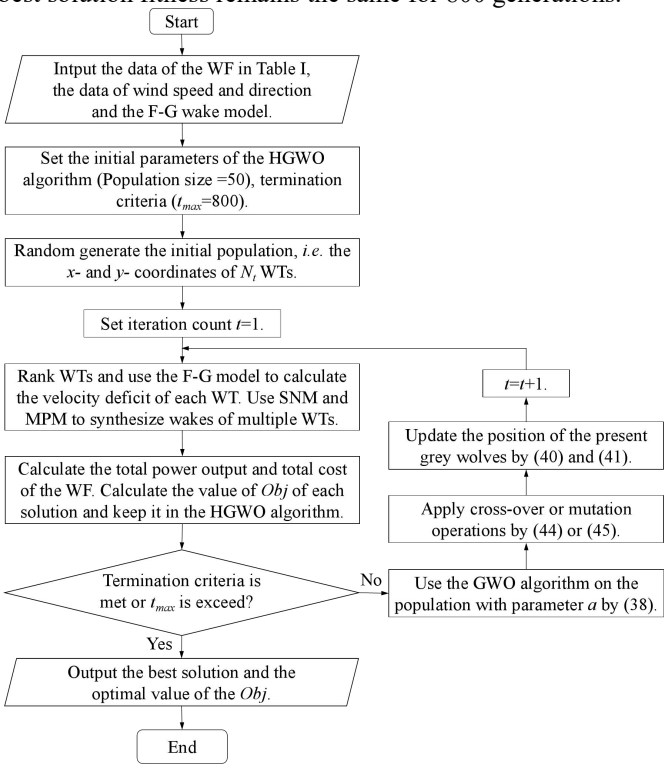

Fig. 12. Application of the HGWO algorithm in the WT optimal micro-siting problem using the F-G wake model.

V. Case Study

The case study takes the WF in the offshore area of a coastal city in Jiangsu Province of China as an example. The necessary simulation parameters of the WF and natural environment are shown in Table I. In this paper, the MM100 WT manufactured by Senvion [39] is assumed to be installed.

TABLE I
Simulation Parameters of the WF

z_h (m) WT Hub Height	r_r (m) WT Rotor Radius	C (MW) WT Capacity	C_T WT Thrust Coefficient	v_{in} (m/s) WT Cut-in Speed
100	50	2	0.88	3
v_r (m/s) WT Rated Speed	v_{out} (m/s) WT Cut-out Speed	ρ (kg/m^3) Air Density	z_0 (m) Surface Roughness Length	U (kV) Internal Voltage
11	22	1.25	0.0002	33
$CAPEX_{WT}$ (M€/MW)	$OPEX_{unit}$ (€/kW/year)	r (%) Discount Rate	N (year) WF Lifetime	T (h) Hours in One Year
3.5	105	5.2	25	8760

In order to test the performance of the F-G wake model in the WT optimal micro-siting problem of the HGWO algorithm, both Jensen's model and the F-G model are used. The optimal micro-siting of various numbers of WTs (N_t=20, N_t=25 and N_t=30) obtained by the HGWO algorithm are depicted in Fig. 13 and the simulation results are given in Table II.

The WF efficiency in Table II is defined by (46).

$$\eta(\%)=\frac{E\left(P_{total}\right)}{E\left(P_{total}^{no\_wake}\right)}\times 100\% \tag{46}$$

where the denominator denotes the ideal expected total output power supposing there is no wake effect.

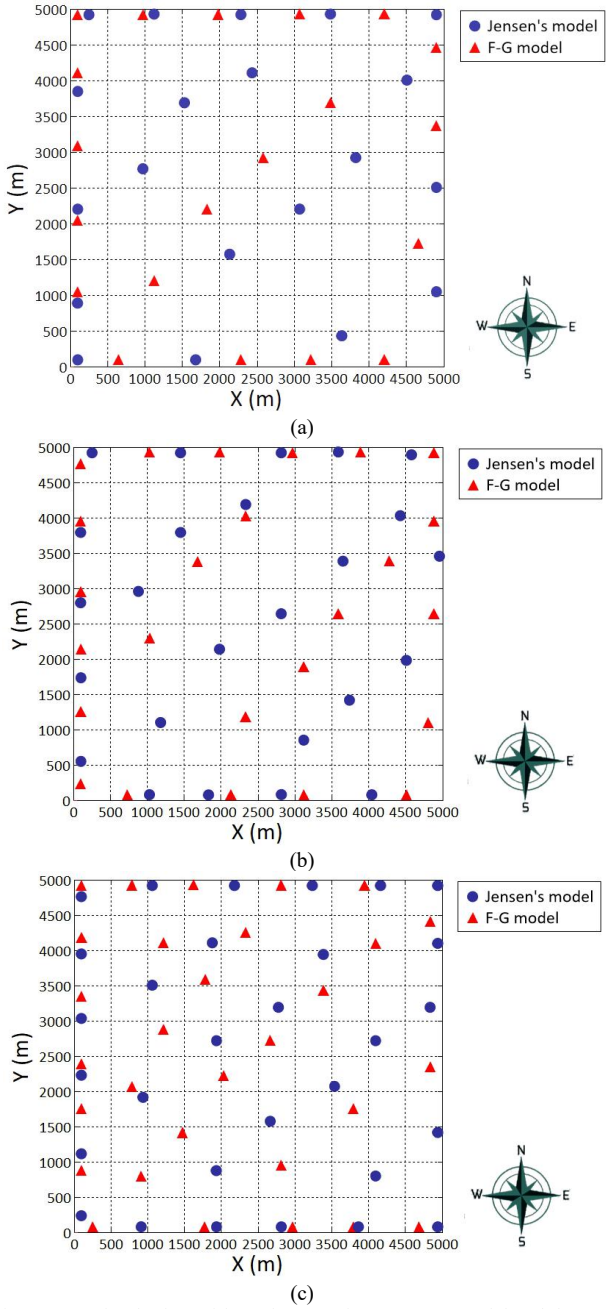

Fig. 13. Optimal micro-siting of WTs using Jensen's model and the F-G model. (a) 20 WTs. (b) 25 WTs. (c) 30 WTs.

Comparing the results in Table II of the optimized layout with the control group in which the WTs are randomly distributed in the WF, the efficiency and the total net power is higher in the optimized layout. It means that the optimization of a WF layout is necessary and vital before its construction.

Generally, the WF efficiency obtained by the HGWO algorithm using the two wake models is in accordance with the reports that the power losses caused by WT wakes are in the range of around 10-20% of the total power output of a WF.

Compared with the optimal power generation using Jensen's model and the F-G model, a decrease in power generation is revealed. The amounts decline from 23021 to 21677 for 20 WTs, from 28160 to 26537 for 25 WTs and from 32916 to 31278 for 30 WTs respectively. The WF efficiency drops from 89.55%, 87.63% and 85.36% to 84.32%, 82.58% and 81.11% for 20, 25, 30 WTs, respectively and the total wake deficits of the WF increases accordingly. It makes sense because as discussed before, Jensen's model underestimates the deficit of wind speed at a specific downwind distance.

Although in general, the predictions of Jensen's model used by the majority of the WF optimization experiments are in fine agreement with the observations, the accuracy of this model for large WFs has been put into question because it systematically underestimates the wake deficits inside large WFs. With the expansion of WF capacity, the calculation error of wake deficits caused by the inaccurate Jensen's model will accumulate and raise to an enormous extent. If the F-G model is applied to the optimal layouts obtained by Jensen's model (*i.e.* the blue circles' locations in Fig. 13) to recalculate the output power of the WF, the simulation results are shown in Table III. It can be clearly seen that the power output of the WTs using the F-G model when they are placed at the red triangles' locations is higher than those using the F-G model at the blue circles' locations and the corresponding objective function value is smaller. Since the F-G model is close to the real wake, this is a clear evidence that the WF layout obtained by using Jensen's model is a sub-optimal solution.

Applying the F-G model in the WT micro-siting optimization process has more accurate and realistic results on the power generation of the WF which will benefit the WF planner to find the best layout. In this way, a large quantity of budget will be saved and more profits will be made for the WF investors. However, as can be inferred from Table II, the weakness of the F-G model is the increase of computational burden, which leads to a longer running time required by the HGWO algorithm to find the optimal solution. Nevertheless, WF layout planning is not done all the time, over and over. Since computation time is cheap nowadays, such an increase of the simulation time is not a big problem, if the application of the F-G model can create a better layout that reduces the cost of wind energy.

In order to test the performance of the HGWO algorithm, it is compared with the GWO algorithm and the GA (case: N_t=30, the F-G model). It can be inferred from Fig. 14 that the HGWO algorithm which is a hybrid algorithm outperforms the other two algorithms not only in the ability of searching for the optimal solution but also in the convergence speed.

TABLE II
SIMULATION RESULTS OF DIFFERENT CASES

Wake Model Type	WTs Number N_t	Objective function *LCOE* (€/MWh)		Total output power $E(P_{total})$ (kW)		Efficiency η (%)		Total wake deficits (%)		Simulation time (s)
		Random layout	Optimized layout	Random layout	Optimized layout	Random layout	Optimized layout	Random layout	Optimized layout	Optimized layout
Jensen's model	20	82.28	71.25	19934	23021	77.54	89.55	22.46	10.45	392
	25	84.17	72.79	24355	28160	75.79	87.63	24.21	12.37	478
	30	86.28	74.67	28501	32916	73.91	85.36	26.09	14.64	843
F-G model	20	83.93	75.56	19517	21677	75.92	84.32	24.08	15.68	713
	25	86.89	77.15	23580	26537	73.38	82.58	26.17	17.42	1102
	30	88.97	78.64	27618	31278	71.62	81.11	28.38	18.89	1497

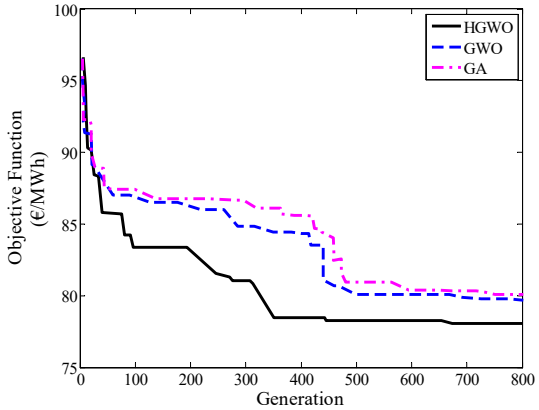

Fig. 14. Convergence characteristics of the HGWO algorithm, the GWO algorithm and the GA.

TABLE III
SIMULATION RESULTS OF THE COMPARISON CASES

Case	WTs Number N_t	Objective function *LCOE* (€/MWh)	Total output power $E(P_{total})$ (kW)	Efficiency η (%)	Total wake deficits (%)
F-G model for blue circles' locations	20	76.81	21332	82.98	17.02
	25	78.35	26139	81.34	18.66
	30	80.69	30460	78.99	21.01

VI. CONCLUSION

The motif of this paper is to seek the optimal positioning of WTs in a large WF. For this purpose, a more accurate wake model, the F-G model has been adopted. The main conclusions can be summarized as below.

a) The motivation of combining Frandsen's model and the Gaussian distribution equations to form the F-G model for WT micro-siting design is illustrated after the indication of the deficiencies of existent popular wake models. The superiority of the F-G model is justified by comparison with other wake models using wind tunnel measurements and LES data.

b) The F-G model is applied in the WT optimal micro-siting problem and solved by the HGWO algorithm. The simulation results show that compared with the cases using Jensen's model, when using the F-G model the WF's efficiency drops and total wake deficits increase accordingly. This is in agreement with the fact that Jensen's model underestimates the wake deficits. The suitability of the F-G model has been successfully demonstrated by analyzing the WT micro-siting problem within large WFs.

c) The HGWO algorithm has the best performance compared with the GA and GWO algorithm in finding the optimal solution and convergence speed. It implies that the HGWO algorithm can be an ideal tool to solve the WT micro-siting

problem.

d) Although this demonstrative case study is taken for an offshore WF, the application of the F-G model based WF optimization can also be used for onshore WFs with suitable parameter adjustments.

e) Future research should be focused on the further validation of the F-G model by conducting real wind field experiments and the inclusion of cabling into the WF optimization framework.

REFERENCES

[1] World Wind Energy Statistics, 2018. [Online]. Available: http://www.wwindea.org/2018-statistics/

[2] J. S. González *et al.,* "A review and recent developments in the optimal wind-turbine micro-siting problem," *Renew. and Sustain. Energy Reviews*, vol. 30, no. 2, pp. 133-144, 2014.

[3] G. Mosetti, C. Poloni, and B. Diviacco, "Optimization of wind turbine positioning in large wind farm by means of a genetic algorithm," *J. Wind Eng. Ind. Aerodynam.*, vol. 51, no.1, pp. 105-116, 1994.

[4] S. Z. Liang, and Y. T. Fang, "Analysis of the Jensen's model, the Frandsen's model and their Gaussian variations," 17th International Conference on Electrical Machines and Systems, Hangzhou, China, pp. 3213-3219, Oct. 22-25, 2014.

[5] N. O. Jensen, "A note on wind generator interaction," *Risø-M-2411*, Risø *National Laboratory*, 1983.

[6] I. Katic, J. Højstrup, and N. O. Jensen, "A simple model for cluster efficiency," *Proceedings of EWEC'86*, Rome, Italy, pp. 407-410, 1986.

[7] R. Shakoor *et al.,* "Wake effect modeling: a review of wind farm layout optimization using Jensen's model," *Renew. and Sustain. Energy Reviews*, vol. 58, pp. 1048-1059, 2016.

[8] S. A. Grady, M. Y. Hussaini, and M. M. Abdullah, "Placement of wind turbines using genetic algorithms," *Renew. Energy*, vol. 30, no. 2, pp. 259-270, 2005.

[9] S. Sisbot *et al.,* "Optimal positioning of wind turbines on Gokceada using multi-objective genetic algorithm," *Wind Energy*, vol. 13, no. 4, pp. 297-306, 2009.

[10] Y. K. Wu *et al.,* "Optimization of the wind turbine layout and transmission system planning for a large-scale offshore wind farm by AI technology," *IEEE Trans. Ind. Appl.*, vol. 50, no. 3, pp. 2071-2080, 2014.

[11] H. Long and Z. J. Zhang, "A two-echelon wind farm layout planning model," *IEEE Trans. Sustain. Energy*, vol. 6, no. 3, pp. 863-871, 2015.

[12] P. Hou *et al.,* "Optimized placement of wind turbines in large-scale offshore wind farm using particle swarm optimization algorithm," *IEEE Trans. Sustain. Energy*, vol. 6, no. 4, pp. 1272-1282, 2015.

[13] Z. Song, Z. J. Zhang, and X. Y. Chen, "The decision model of 3-dimensional wind farm layout design," *Renew. Energy*, vol. 85, pp. 248-258, 2016.

[14] H. J. Yang *et al.,* "Wind farm layout optimization and its application to power system reliability analysis," *IEEE Trans. Power Syst.*, vol. 31, no. 3, pp. 2135-2143, 2016.

[15] P. Hou *et al.,* "Offshore wind farm layout design considering optimized power dispatch strategy," *IEEE Trans. Sustain. Energy*, vol. 8, no. 2, pp. 638-647, 2017.

[16] H. Long *et al.,* "Formulation and analysis of grid and coordinate models for planning wind farm layouts," *IEEE Access*, vol. 5, pp. 1810-1819, 2017.

[17] R. J. Barthelmie *et al*., "Comparison of wake model simulations with offshore wind turbine wake profiles measured by sodar," *J. Atmospheric Ocean Technol.* vol. 23, pp. 881-901, 2005.

[18] GH WindFarmer theory manual. Garrad Hassan and Partners Ltd., 2009.

[19] G. Crasto *et al.,* "Wake modeling with the actuator disc concept," *Energy Procedia*, vol. 24, pp. 385-392, 2012.

[20] version 1.3 ed. Openwind theoretical basis and validation. AWS Truepower, LCC, 2010.

[21] G. C. Larsen, A simple wake calculation procedure. Risø National Laboratory, 1988.

[22] S. Frandsen *et al.,* "Analytical modelling of wind speed deficit in large offshore wind farms," *Wind Energy*, vol. 9, no. 1, pp. 39-53, 2006.

[23] J. S. González, M. B. Payán, and J. R. Santos, "A new and efficient method for optimal design of large offshore wind power plants," *IEEE Trans. Power Syst.*, vol. 28, no. 3, pp. 3075-3084, 2013.

[24] T. Ishihara, A. Yamaguchi, and Y. Fujino, "Development of a new wake model based on a wind tunnel experiment," *Global Wind Power*, pp. 28-31, 2004.

[25] X. L. Yang and F. Sotiropoulos, "Analytical model for predicting the performance of arbitrary size and layout wind farms," *Wind Energy*, vol. 19, no. 7, pp. 1239-1248, 2016.

[26] M. Bastankhah and F. Porté-Agel, "A new analytical model for wind-turbine wakes," *Renew. Energy*, vol. 70, pp. 116-123, 2014.

[27] L. L. Tian *et al.,* "Development and validation of a new two-dimensional wake model for wind turbine wakes," *J. Wind Eng. Ind. Aerodyn.*, vol. 137, pp. 90-99, 2015.

[28] X. X. Gao, H. X. Yang, and L. Lu, "Optimization of wind turbine layout position in a wind farm using a newly-developed two-dimensional wake model," *Appl. Energy*, vol. 174, pp. 192-200, 2016.

[29] K. Emrah, "Aerodynamics of wind turbines," in Fundamental and Advanced Topics in Wind Power, C. Rupp, Ed., Croatia: InTech, pp. 1-18, June, 2011.

[30] Y. T. Wu and F. Porté-Agel, "Atmospheric turbulence effects on wind-turbine wakes: an LES study," *Energies*, vol. 5, no. 12, pp. 5340-5362, 2012.

[31] Megavind. Megavind LCOE Model-guidelines and documentation, 2015. [Online]. Available: https://megavind.windpower.org/download/2452/1500318_documentation_and_guidelinespdf

[32] P. E. Réthoré *et al.,* "TOPFARM: Multi-fidelity optimization of wind farms," *Wind Energy*, vol. 17, pp. 1797-1816, 2014.

[33] X. Gong, S. Kuenzel, and B. C. Pal, "Optimal wind farm cabling," *IEEE Trans. Sustain. Energy*, vol. 9, no. 3, pp. 1126-1136, 2018.

[34] A. Feijóo, and D. Villanueva, "Wind farm power distribution function considering wake effects," *IEEE Trans. Power Syst.*, vol. 32, no. 4, pp. 3313-3314, 2017.

[35] National Meteorological Information Center, 2018. [Online]. Available: http://data.cma.cn/data/detail/dataCode/A.0012.0001.html

[36] M. A. Lackner and C. N. Elkinton, "An analytical framework for offshore wind farm layout optimization," *Wind Eng.*, vol. 31, no. 1, pp. 17-31, 2007.

[37] R. Sanjay *et al.*, "Optimal allocation of distributed generation using hybrid grey wolf optimizer," *IEEE Access*, vol. 5, pp. 14807-14818, 2017.

[38] Z. J. Teng, J. L. Lv, and L. W. Guo, "An improved hybrid grey wolf optimization algorithm," Soft Computing. *Springer*, pp. 1-15, 2018.

[39] Technical data MM100, 2019. [Online]. Available: https://www.senvion.com/global/en/products-services/wind-turbines/mm/mm100/

Siyu Tao (S'18) received the B.Sc degree in electrical engineering from Zhejiang University, China in 2013 and the M.Sc degree in control systems from Imperial College London, U.K. in 2014. She is currently pursuing the Ph.D degree at the Department of Electrical Engineering, Southeast University, China. Her research interests include wind energy and power systems.

Stefanie Kuenzel (S'11-M'14) received the Ph.D. degree from Imperial College London, U.K. in 2014. She is currently the Head of the Power Systems group and Lecturer with the Department of Electronic Engineering, Royal Holloway, University of London. Her research interests include renewable generation, smart metering and transmission, including HVDC.

Qingshan Xu (M'09) received the Ph.D degree in electrical engineering from Southeast University, China in 2006. He was a Visiting Scholar of the Aichi Institute of Technology, Japan, from 2007 to 2008. He is currently a professor with the Department of Electrical Engineering, Southeast University, China. His research interests include renewable energy and power system operation and control.

Zhe Chen (M'95-SM'98-F'19) received the Ph.D. degree in electrical engineering from University of Durham, Durham, U.K, in 1997. He is a full Professor with the Department of Energy Technology, Aalborg University, Denmark. He is the Leader of Wind Power System Research Program, Department of Energy Technology, Aalborg University and the Danish Principle Investigator for Wind Energy of Sino-Danish Centre for Education and Research. His research interests include power systems, power electronics and electric machines, wind energy, and modern power systems.